Malaysian Catalysis-An International Journal

Malay. Catal.Int.J Vol 1, Issue 2 (2021) 01-11

ARTICLE TYPE

Synthesis of MnO_2 Particles via One Step Localized Heating Method as Catalyst for Dye Degradation

S.L.Chiam, S. Y. Pung*[a.]

[a] School of Materials and Mineral Resources Engineering, Engineering Campus, Universiti Sains Malaysia, 14300 Nibong Tebal, Pulau Pinang, Malaysia

Received 5th Oct 2021,
Revised 3rd Dec 2021,
Accepted 6th Dec 2021

DOI: 10.22452/mcij.vol1no2.1

Corresponding author:
sypung@usm.my

Abstract

This work demonstrated the synthesis of MnO_2 particles via a rapid one-step localized heating method. The heat was transferred directly from the wire into the precursor solution, minimizing the heat loss to the surrounding. As a result, the precursor solution was heated up rapidly and MnO_2 particles with different morphologies were successfully synthesized in a short duration within 10 to 15 min. These MnO_2 particles were used as catalysts in the degradation of Rhodamine B (RhB) organic dye. Particularly, MnO_2 particles synthesized at 10 min possessed outstanding catalytic activity with 99% degradation efficiency of RhB dye in 10 min of reaction time. This was significantly contributed by its 3D nanoflowers morphology, which provided more active sites for catalytic activities. The promising catalytic activity, synthesizing by a simple and affordable synthesis setup could provide an alternative in developing MnO_2 catalyst for organic pollutants removal.

Keywords: Manganese dioxide (MnO_2), nanoflowers; catalyst; dye degradation; rapid synthesis

1.0 Introduction

MnO_2, which is categorized as n-type semiconductor, possesses band gap energy in the range of 1–2 eV [1]. It is one of the promising candidates in the removal of organic dye [2-4]. It possesses various redox activities due to its different oxidation states (+2, +3 and +4), low toxicity, and abundancy. These unique properties make it an attractive potential catalyst for wastewater treatment [5, 6]. In addition, MnO_2 particles are approximately 75% cheaper than the commonly used photocatalyst, for example TiO_2 particles. One kilogram of MnO_2 particles costs USD 600 whereas one kilogram of TiO_2 particles will need USD 2850 (information obtained from www.sigmaaldrich.com).

Numerous approaches have been reported in the synthesis of MnO_2 particles such as hydrothermal [7], sol-gel [1], wet chemical [8], precipitation [9], microwave [10], ice-templating [11], reflux [12] and mechanochemical process [13]. Among these methods, hydrothermal, sol-gel, and precipitation are frequently reported in the synthesis of MnO_2 particles. Their synthesis processes are simple, easy to repeat, and the size and morphology can be easily tailored by changing the reaction's parameters. However, attributed to their setups, these methods usually require relatively lengthy synthesis time (>8 h) and high usage of electrical energy (>200 W h) [14]. These methods are considered inefficient in terms of energy and time as the heat generated by the heating coils is transferred externally from the reactor system to the precursor solution. Most of the heat is lost during this process. This became the main drawback for practical application which require mass production at a low cost of synthesis

A rapid synthesis of MnO_2 particles via the localized heating (LH) method is reported in this paper. Once the electric current was passed through the wire, the heat was generated and was transferred directly to the target solution. This approach minimizes the heat lost to the surrounding. With this, high heating rate was attained and MnO_2 particles were successfully produced in a short duration (10 min) with low usage of electrical energy (≈ 40W h). The MnO_2 particles demonstrated promising catalytic activity attributed to their 3D nanoflowers morphology that offered a large surface area for dye removal.

2.0 Materials and Methods

2.1 Synthesis of MnO_2 particles

The precursor solution was prepared using a 2:3 molar ratio of $KMnO_4$ (0.70 g) and $MnSO_4$ (1.125 g) which dissolved in distilled water (80 ml). A benchtop power regulator was used to pass the electrical current to the wire that submerged in the precursor solution under constant stirring. The temperatures of the wire and the precursor solution were monitored by thermocouples. The particles collected were then washed with ethanol and distilled water before drying at room temperature. The effect of heating duration was studied.

2.2 Materials Characterization

Field emission scanning electron microscopy (FESEM, Zeiss Supra 35 VP) and Tecnai G2 F20 X-Twin transmission electron microscope (TEM) were used to study the surface morphologies of the particles. X-ray diffraction (XRD) analysis using a D8 Advance (Bruker, Karlsruhe, Germany) automated X-ray diffractometer system was used to identify the crystal phases of the particles. UV-Visible spectroscopy (Varian Cary 50) was used to study the catalytic activity of the particles.

2.3 Catalytic removal of RhB dye

MnO_2 particles (0.025 g) were added into the beaker filled with RhB solution (250 ml, 2.5 mg/L). At given time intervals, the mixed solution (2.5 ml) was collected. The absorbance of solution collected at different time intervals was measured by UV-Vis spectrometer. The degradation efficiency was calculated from the absorption of RhB at 554 nm using **Eq. 1.**

$$\text{Removal efficiency (\%)} = \frac{A_o - A_t}{A_o} \times 100 \qquad (1)$$

where A_o and A_t is the absorbance of RhB aqueous solution at t=0 min and after t min of reaction respectively. The kinetics of the degradation process were calculated based on the pseudo-first-order kinetic model using **Eq. 2**.

$$\ln(A_0/A_t) = kt \qquad (2)$$

where A_o and A_t are the concentration of RhB at t=0 min and after t min of reaction respectively.

3.0 Results and discussion

Figure 1 illustrates the XRD profiles of the particles synthesized at a heating duration of 10 and 15 min. The XRD profiles show a similar diffraction pattern where there are five broad diffraction peaks detected at 11.59 °, 23.76 °, 37.23 °, 42.08 °and 66.69 ° corresponding to (110), (220), (211), (031) and (002) crystal planes of MnO_2 (JCPDS 44-141). Besides, both profiles display broad diffraction peaks. This suggests that the MnO_2 particles possessed amorphous structures.

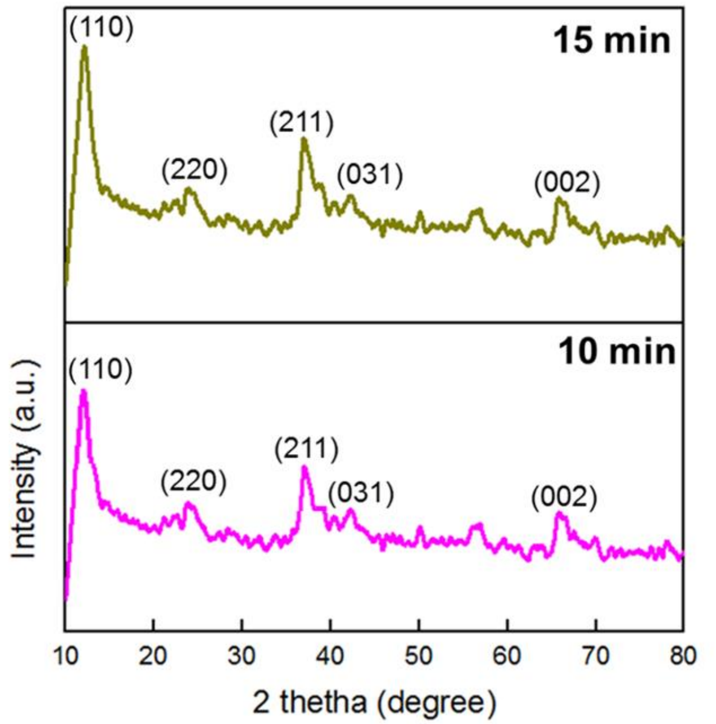

Figure 1: XRD profiles of MnO_2 particles synthesized at different heating duration.

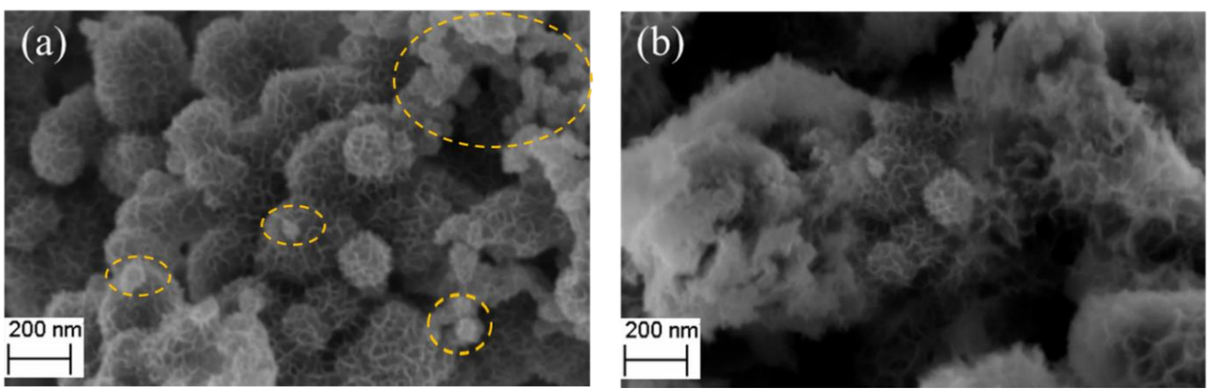

Figure 2: FESEM images of MnO_2 particles synthesized at heating duration of (a) 10min (circled area represent small particles) and (d) 15 min at a magnification of 30K .

Figures 2a and b illustrate the morphologies of MnO_2 particles synthesized at a heating duration of 10 and 15 min. The MnO_2 particles possessed different morphologies in general. At 10 min, hierarchical flower-like structures was formed. These flower-like particles were made up of assemblies of thin intersected nanosheets. Besides, tiny particles were found deposited on the surface of MnO_2 nanoflowers as highlighted in the yellow circle. By increasing the heating duration to 15 min, agglomerated structures were observed over the surface of MnO_2 particles.

The growth mechanism of MnO_2 particles using the LH method is proposed in Figure 3. As illustrated in Figure 3a, the temperature of wire and solution was 28 °C at t=0 min. Since there was no current supply, no heat was generated from the wire. Therefore, no MnO_2 particles were synthesized. After switching for 10 min, the temperature of the wire reached 85 °C while the temperature of the adjacent precursor solution was 80 °C. This observation suggests that heat transferred rapidly into the precursor solution. This is explainable as LH method allowed the transfer of heat constantly and directly into the precursor solution. This offered more efficient energy transfer and thus high heating rate. The temperature of the precursor solution was sufficient to initiate the redox reaction between $KMnO_4$ and $MnSO_4$. According to Classic Nucleation Theory (CNT), under high heating rate, nucleation reaction will be triggered within a short time. This in turn would offer a higher concentration of nucleus. The MnO2 nuclei formed in the precursor solution would self-assembly and grow into crumpled and intersected nanoflowers as shown in Figure 2a. Besides, secondary nucleation could also occur under rapid heating rate conditions [15, 16]. Small particles were formed and deposited on the surface of MnO2 nanosheets.

Most of the precursor in the solution was depleted when the heating duration was prolonged to 15 min. Subsequently, a slower nucleation rate was observed. Meanwhile, Ostwald ripening occurred in the solution that was heated under uniform temperature. This phenomenon was frequently seen in the solid-solutions medium where the small crystals redeposit onto a larger crystal over time as observed in Figure 2b.

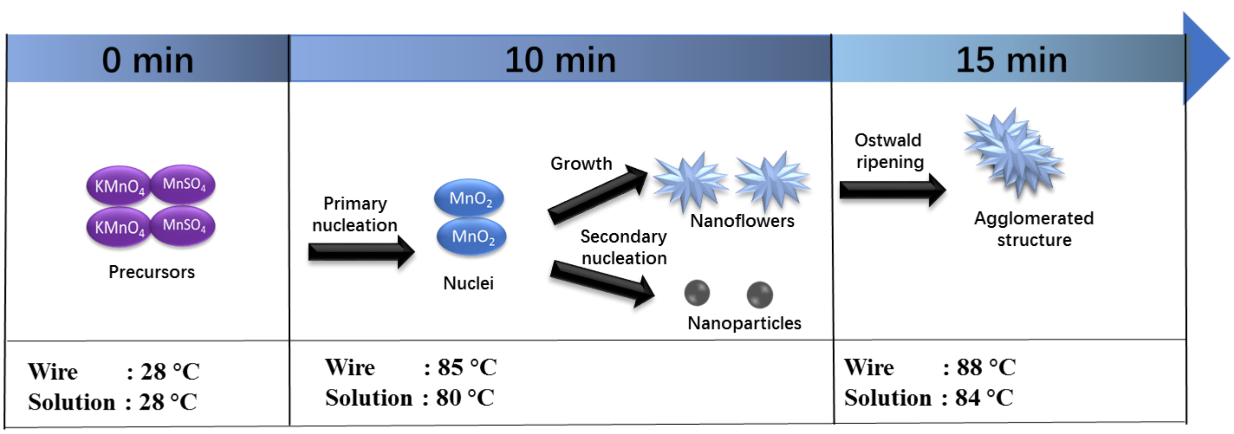

Figure 3: A schematic diagram illustrates the morphology evolution of MnO_2 particles nanoflowers with heating durations.

The catalytic activities of MnO_2 particles were investigated by assessing their removal efficiency towards the RhB dye. The UV–Vis profiles of RhB dye with MnO_2 particles synthesized at 10 min and 15 min are shown in Figure 4. Both the characteristic peaks of RhB at the wavelength of 554 nm decreased with time. The distinct peaks of MnO_2 particles synthesized at 10 min reduced faster than those synthesized at 15 min. The relative intensity of the absorption peaks for MnO_2 synthesized at 10 min vanished entirely after 20 min of reaction time.

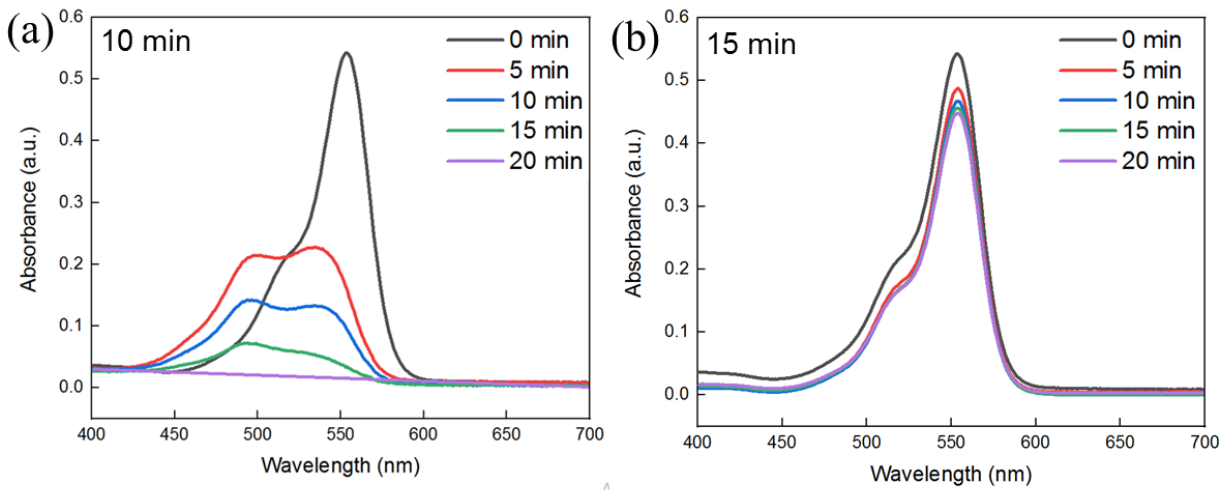

Figure 4: UV–Vis absorption profile of RhB as a function of reaction time using MnO_2 particles synthesized at (a) 10 min and (b) 15 min.

The characteristic absorbance peak of RhB is 554 nm. The decrease of absorbance at 554 nm indicates that the reduction of RhB concentration in solution. The removal of RhB from the solution could be via degradation, adsorption or a combination of both mechanisms. MnO_2 particles synthesized at 10 min displayed a blue shift in the wavelength. The wavelength was shifted from 554 nm to 449 nm suggests the degradation of RhB molecules via the formation of nitrogen-centered radicals, which underwent a two-step reaction of N-deethylation followed by the destruction of the backbones. Thus, this is solid evidence that the removal of RhB by MnO_2 particles synthesized at 10 min was through the degradation process. On the contrary, no apparent band shift was observed when using MnO_2 particles synthesized at 15 min. As both MnO_2 particles were synthesized using the same process, except synthesis duration, thus it is strongly believed that the removal of RhB by MnO_2 particles synthesized at 15 min was also through the degradation process. Nevertheless, the degradation process was much slower than MnO_2 synthesized at 10 min. Thus, the shifting of absorbance peak was not observed during the photocatalytic test.

A plot of removal efficiency of RhB with time is demonstrated in Figure 5a using Eq. 1 to evaluate their catalytic activities quantitatively. The self-degradation of RhB is negligible as it is less than 1.0%. The degradation efficiency of MnO_2 particles synthesized at 10 min and 15 min were 99 % and 17 % respectively. The kinetics of the degradation process of RhB by MnO_2 particles were explored. The linear fittings in Figure 5b indicated that the degradation of RhB by these MnO_2 particles followed the pseudo-first order kinetic model. The reaction rate constants of MnO_2 particles synthesized at 10 min and15 min were 0.162 and 0.010 min− 1 respectively. The MnO_2 particles synthesized at 10 min possessed the highest removal efficiency. Its efficiency is approximately 6 folds more elevated than MnO_2 synthesized at 15 min.

Next, the repeatability test on the catalytic performances of MnO_2 particles synthesized at 10 min in subsequent five cycles are shown in (Figure 5c). MnO_2 particles can maintain their catalytic efficiency up to 70% after reusing for five cycles. It can be concluded that the outstanding catalytic activity of MnO_2 particles synthesized at 10 min was significantly contributed by its hierarchical flower-like morphology that provided more active sites for catalytic activities to occur. According to a previously reported study, 3D nanoflowers in a minute structure provided a high surface area to volume ratio, which increased the chance of adsorption of dye molecules, providing a high rate of reaction and hence high removal rate on RhB dye [17, 18].

Lastly, the catalytic performance of MnO_2 particles synthesized at 10 min was compared with other MnO_2 based catalysts reported recently. The synthesized MnO_2 catalyst outperformed other reported catalysts. Besides, the synthesis duration is the shortest, proving its feasibility for practical application.

Table 1: Catalytic activity of MnO_2 based catalyst in RhB dye degradation reported in the literature

Catalyst	Synthesis method	Synthesis duration (hr)	Target pollutant/ concentration (mg/L)	Catalyst concentration (g/L)	Reaction time (min)	Removal efficiency (%)	Activator	Ref
MnO_2/SiO_2 core-shell	Mixing & calcination	6	RhB / 5.0	0.5	90	84.9	Acid	[19]
Amorphous MnO_2	Mechanochemical	5	RhB / 9.5	0.16	30	99	UV light & acid	[20]
MnO_2/ carbon aerogel	Hydrothermal	2	RhB / -	1.5	80	99.5	H_2O_2	[21]
$MnO_2/Mn_3O_4/$ Fe_3O_4	Hydrothermal	6	RhB / 10.0	0.015	130	94.5	Visible light	[22]
αMnO_2/ Palygonskite	Hydrothermal	8	RhB / 20.0	0.1	180	100	PMS & Acid	[2]
MnO_2 particles	Localized heating	0.16	RhB / 2.5	0.1	20	99	Acid	**This work**

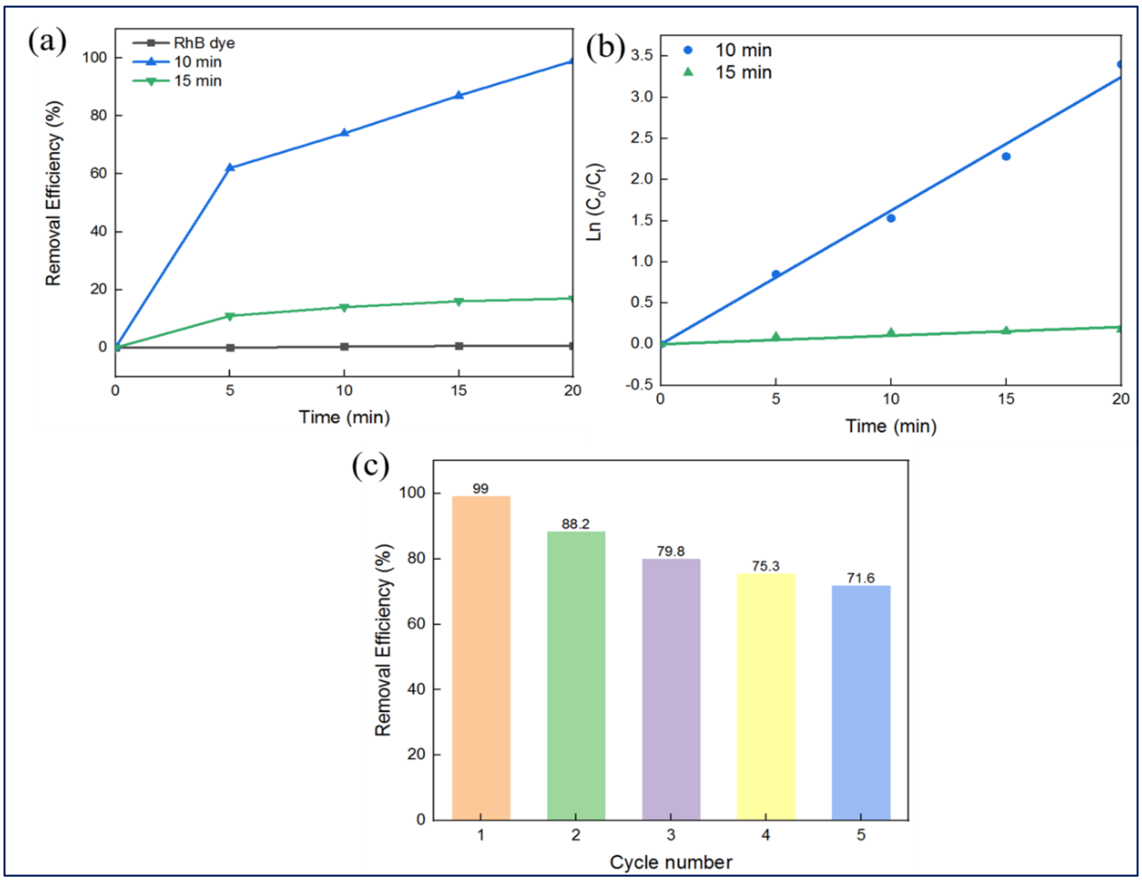

Figure 5: (a) Removal efficiency, (b) rate of removal and (c) repeatability test (10 min) of MnO_2 particles.

Conclusion

In summary, the synthesis of MnO_2 particles could be achieved in a short duration of 10 min using the one-step localized heating method. The underlying mechanism for the formation of MnO_2 particles followed to Classical Nucleation Theory. It involved nucleation of precursors, followed by the growth of flower-like MnO_2 particles. Besides, tiny particles due to secondary nucleation were deposited on the surface of MnO_2 particles. Meanwhile, prolonging the heating duration led to Ostwald ripening, resulting in the formation of agglomerated structure. The practical application of these MnO_2 particles was tested by measuring their catalytic activity on the degradation of RhB organic dye. The MnO_2 particles synthesized at 10 min possessed the best catalytic activity. Besides, they could re-use at least cycles with efficacy maintained up to 70 %. The outstanding catalytic activity of these MnO_2 could be attributed to their unique 3D nanoflowers morphology, which provided a large surface area to volume ratio for a catalytic activity to occur. This work presents a simple, facile, and efficient synthesis route for MnO_2 particles.

Acknowledgments

The authors acknowledge the research funding (RUI USM 1001/PBAHAN/ 8014095) from Universiti Sains Malaysia.

Competing interests

The authors declare no competing of interest.

References

1. Y.L. Chan, S.Y. Pung, S. Sreekantan, F.Y. Yeoh, Photocatalytic activity of β-MnO_2 nanotubes grown on PET fiber under visible light irradiation. *J. Exp. Nanosci.* **2016**, 11(8), 603-618.
2. C. Huang, Y. Wang, M. Gong, W. Wang, Y. Mu, Z.H. Hu, α-MnO2/Palygorskite composite as an effective catalyst for heterogeneous activation of peroxymonosulfate (PMS) for the degradation of Rhodamine B. *Sep. Purif. Technol*, **2020,** 230, 115877.
3. X. Bi, Y. Huang, X. Liu, N. Yao, P. Zhao, X. Meng, D. Astruc, Oxidative degradation of aqueous organic contaminants over shape-tunable MnO2 nanomaterials via peroxymonosulfate activation. *Sep. Purif. Technol.*, **2021,** 119141.
4. M. Cao, Z. Zhuang, Y. Liu, Z. Zhang, J. Xuan, Q. Zhang, W. Wang, Peptide-mediated green synthesis of the MnO2@ ZIF-8 core-shell nanoparticles for efficient removal of pollutant dyes from wastewater via a synergistic process. *J. Colloid Interface Sci*, **2021,** *In-press*

5. C. Fang, H. Gujarati, F. Osinaga, V. Hsia, M.A. Cheney, M.K. Kharel, Optimization of the catalytic activity of manganese dioxide (MnO2) nanoparticles for degradation of environmental pollutants. *Res. Chem. Intermed*, **2021**, 1-18
6. R. Qu, X. Li, Y. Wei, L. Feng, A bifunctional β-MnO2 mesh for expeditious and ambient degradation of dyes inactivating peroxymonosulfate (PMS) simultaneous oil removal from water. J. Colloid Interface Sci., 579, **2020**, 412-424
7. L. Xiao, W. Sun, X. Zhou, Z. Cai, F. Hu, Facile synthesis of mesoporous MnO_2 nanosheet and micro flower with efficient photocatalytic activities for organic dyes. *Vacuum*, **2018,** 156, 291-297.
8. P. Xia, B. Zhu, B. Cheng, J. Yu, J. Xu, 2D/2D g-C_3N_4/MnO_2 nanocomposite as a direct Z-scheme photocatalyst for enhanced photocatalytic activity. *ACS Sustain. Chem. Eng.* **2018**. 6(1), 965-973.
9. J. Chen, Z. Huang, H. Meng, L. Zhang, D. Ji, J. Liu, Z. Li, A facile fluorescence lateral flow biosensor for glutathione detection based on quantum dots-MnO_2 nanocomposites. *Sens. Actuators, B: Chem.* **2018,** 260, 770-777.
10. Z. Ai, L. Zhang, F. Kong, H. Liu, W. Xing, J. Qiu, J. Microwave-assisted green synthesis of MnO_2 nanoplates with environmental catalytic activity. *Mater. Chem. Phys.*, **2008**, 111(1), 162-167.
11. H. Sun, Y. Shang, K. Xu, Y. Tang, J. Li, Z. Liu, MnO_2 aerogels for highly efficient oxidative degradation of Rhodamine B. *Rsc Adv.* **2017**, 7(48), 30283-30288.
12. H.J. Cui, H. Z. Huang, B. Yuan, M.L. Fu, Decolorization of RhB dye by manganese oxides: effect of crystal type and solution pH. *Geochem. Trans*. **2015**, 16(1), 1-8.
13. T.K. Achar, A. Bose, P. Mal, Mechanochemical synthesis of small organic molecules. *Beilstein J. Org. Chem.* **2017**, 13(1) 1907-1931.
14. E.J. Kim, D. Oh, C.S. Lee, J. Gong, J. Kim, Y.S. Chang, Manganese oxide nanorods as a robust Fenton-like catalyst at neutral pH: crystal phase-dependent behavior. *Catal. Today*., **2017**, 282, 71-76.
15. Y. Yuan, S.M. Wood, K. He, W. Yao, D. Tompsett, J. Lu, R. S. Yassar, Atomistic insights into the oriented attachment of tunnel-based oxide nanostructures. *ACS nano.,* **2016,** 10(1), 539-548.
16. W. Yao, Y. Yuan, H.A. Ardakani, Z. Huang, F. Long, C.R. Friedrich, R. S. Yassar, Energy-driven surface evolution in beta-MnO_2 structures. *Nano Res.,* **2018**. 11(1), 206-215.
17. M.A. Alheety, S.A. Al-Jibori, A. Karadağ, H. Akbaş, M.H. Ahmed, A novel synthesis of MnO_2 nanoflowers as an efficient heterogeneous catalyst for oxidative desulfurization of thiophenes. *Nano-Struc. Nano-Objects*., **2019. 20**, 100392.
18. R. Yuan, Z. Jiang, Z. Wang, S. Gao, Z. Liu, M. Li, G. Boczkaj, Hierarchical MnO_2 nanoflowers blooming on 3D nickel foam: A novel micro-macro catalyst for peroxymonosulfate activation. *J. Colloid Interface Sci.* **2020**. 571, 142-154.
19. W. Gong, X. Meng, X. Tang, P. Ji, Core-shell MnO2-SiO2 nanorods for catalyzing the removal of dyes from water. *Catalysts,* 7(1), **2017,** 19

20. A. Gagrani, J. Zhou, T. Tsuzuki, Solvent free mechanochemical synthesis of MnO_2 for the efficient degradation of Rhodamine-B. *Ceram.* 44(5), **2018,** 4694-4698

21. H. Wan, H. Ge, L. Zhang, T. Duan, CS@ MnO_2 core-shell nanospheres with enhanced visible-light photocatalytic degradation. *Mater. Lett*, **2019,** 237, 290-293

22. M. Ma, Y. Yang, Y. Chen, F. Wu, W. Li, P. Lyu, W. Huang, Synthesis of hollow flower-like $Fe_3O_4/MnO_2/Mn_3O_4$ magnetically separable microspheres with valence heterostructure for dye degradation. *Catalysts*, **2019**, 9(7), 589